

Effects of Rotation Rates on Microstructure, Mechanical Properties, and Fracture Behavior of Friction Stir-Welded (FSW) AZ31 Magnesium Alloy

J. YANG, D. WANG, B.L. XIAO, D.R. NI, and Z.Y. MA

Three rotation rates were selected for friction stir welded (FSW) rolled AZ31 plates, at a constant welding speed of 100 mm/minutes. As the rotation rate was increased from 800 and 2000 to 3500 rpm, the nugget shape varied from a basin- or ellipse-shaped homogeneous structure to a two-layer structure. The grain characteristic was similar in the nugget zones (NZs) at 800 and 2000 rpm, with the column-rotated basal plane. However, at 3500 rpm, the equiaxed fine grains and column-rotated basal plane were found in the lower zone of the two-layer structure, while elongated coarse grains and the basal plane with little inclination comparable to that in the parent material (PM) were detected in the upper zone. Tensile tests indicated that the fracture behaviors of the FSW AZ31 joints at 800 and 2000 rpm were similar with the weak zones being located at the NZ middle and along the boundary between the NZ and the thermo-mechanically affected zone, while contrasting fracture features were found at 3500 rpm. The ultimate tensile strength (UTS) of the joints increased as the rotation rate increased, with the highest UTS being about 95 pct of the PM at 3500 rpm. The variations in the strength and fracture behavior of the joints with the rotation rate were accounted for by the variation in the texture.

DOI: 10.1007/s11661-012-1373-4

© The Minerals, Metals & Materials Society and ASM International 2012

I. INTRODUCTION

MAGNESIUM alloys are the lightest structural alloys that are commercially available. Nowadays, magnesium alloys have gained huge interest in the aircraft and automobile industries because of the need of weight reduction. Therefore, a reliable welding process is required to support these applications. However, conventional fusion welding has some problems, such as porosity, oxidization, a wide heat-affected zone, and high residual stress, which limit the use of the magnesium alloys.

Friction stir-welding (FSW), a solid joining method,^[1] can eliminate the welding problems in conventional fusion welds, and therefore has been successfully used to weld various magnesium alloys, such as Mg-Al-Zn alloys,^[2-12] Mg-Zn-Y alloys,^[13,14] and Mg-Al-Ca alloy.^[15] Among these magnesium alloys, AZ31, a widely used wrought magnesium alloy, has been widely subjected to FSW investigations.^[2-12] These studies can be classified into two categories. Some studies were focused on the mechanical properties of FSW joints.^[2-9] The others paid attention to the texture variation and material flow patterns during FSW.^[10-12]

In the early studies of FSW AZ31,^[2-4] the optimization of welding parameters was an important issue.

Most studies were conducted on AZ31-H24 plates, and joint efficiencies ($UTS_{\text{Joint}}/UTS_{\text{PM}}$) in the range of 60-85 pct were obtained by changing the rotation rate and welding speed.^[2,3] However, among these studies,^[2-4] there was no concordant conclusion on the relationship between the mechanical properties and the rotation rate and welding speed. Later, Commin *et al.*^[5] found that the joint properties were related to the heat input, and high heat input was favorable for good joint properties. Afrin *et al.*^[6] and Wang *et al.*^[7] reported that the ultimate tensile strength (UTS) of the FSW joints increased as the rotation rates increased from 500 to 1500 rpm for both the H24 and hot-rolled AZ31. Furthermore, Yang *et al.*^[9] found that higher UTS was obtained with a larger diameter shoulder because of greater heat input.

The texture of the magnesium alloys is sensitive to severe plastic deformation because the number of independent slip systems in the hexagonal close packed (HCP) structure is limited.^[16] Park *et al.*^[17] observed a strong texture development in FSW AZ61 and suggested that the basal plane was roughly aligned with the pin surface in the nugget zone (NZ). A similar result was also found in the FSW AZ31 by Woo *et al.*^[10] Besides, the fracture location of the joints was usually located at the thermo-mechanically affected zone (TMAZ), which was attributed to the texture development.^[10,18] Moreover, Suhuddin *et al.*^[11] investigated the grain structure development in the NZ using the electron back-scattered diffraction (EBSD), and found that the material flow varied in the upper and lower parts of the NZ.

For the FSW AZ31 joints, the welding parameters, especially the rotation rate, were found to have

J. YANG, Postgraduate, D. WANG, Assistant Professor, B.L. XIAO and Z.Y. MA, Professors, and D.R. NI, Associate Professor, are with the Shenyang National Laboratory for Materials Science, Institute of Metal Research, Chinese Academy of Sciences, Shenyang 110016, P.R. China. Contact e-mail: zyma@imr.ac.cn

Manuscript submitted January 21, 2012.

Article published online August 22, 2012

significant effects on the mechanical properties,^[2-9] and the texture was reported to influence the mechanical behavior.^[9,10,19] However, the studies on the texture distribution were almost based on a single parameter, without considering the effects of different parameters. On the other hand, many researchers studied the mechanical properties of the joints at varied parameters, but ignored the texture differences. Furthermore, although the mechanical properties of the FSW AZ31 joints were found to increase with the rotation rate,^[5-8] most studies were conducted at rotation rates of 600-2500 rpm, and no attempt had been made to evaluate the FSW AZ31 joints at even higher rotation rates.

In this study, rolled AZ31 plates were friction stir welded at a wide range of rotation rates with the highest rotation rate of 3500 rpm, and the joints were subjected to detailed microstructural examinations and mechanical property evaluations. The aim is to establish the relationship between the rotation rate, texture distribution, and mechanical properties.

II. EXPERIMENTAL

Hot-rolled AZ31 plates with a thickness of 6.3 mm were used in this study. A simple FSW tool was used with a concave shoulder 24 mm in diameter, and a cylindrical threaded pin 8 mm in diameter and 5.9 mm in height. FSW was conducted along the rolling direction (RD) at a welding speed of 100 mm/minutes with a tool tilt angle of 2.8°. Three different rotation rates were used, *i.e.*, the low rate of 800 rpm, the medium rate of 2000 rpm, and the high rate of 3500 rpm, and the FSW joints were, respectively, denoted as the 800 rpm-joint, 2000 rpm-joint, and 3500 rpm-joint in this study (Table I). The principal directions of FSW geometry are denoted as the RD, transverse direction (TD), and normal direction (ND).

The specimens for microstructure examinations were cut perpendicular to the RD. Microstructure characterization and analysis were carried out by optical microscopy (OM), scanning electron microscopy (SEM, Hitachi S-3400N), and electron backscattered diffraction (EBSD, HKL). The OM specimens were etched by means of a corrosive reagent (4.2 g picric acid, 10 ml acetic acid, 10 ml H₂O, and 70 ml ethanol). The specimens for EBSD were prepared by electropolishing using commercial AC2 polishing solution.

The hardness profiles of the transverse cross section along the mid-thickness of the plate were measured using a Vickers hardness tester with a 300-g load for 10 seconds. Transverse tensile specimens with a gauge length of 40 mm and a gage width of 10 mm were

machined, and tested at a strain rate of $1 \times 10^{-3} \text{ s}^{-1}$ using a Zwick/Roell Z050 tester. Besides, mini-sized tensile specimens, each with a gauge length of 10 mm, a gauge width of 2.2 mm, and a gauge thickness of 1.7 mm, were cut in the upper and lower parts of the NZ in the transverse direction for the 3500 rpm-joint, with the gauge center at the weld centerline, and were tested at a strain rate of $1 \times 10^{-3} \text{ s}^{-1}$ using an Instron 5848 tester. The results of tensile tests were taken from three and five specimens, respectively, for the transverse and mini tensile tests. The fracture surfaces of the transverse tensile specimens were observed using SEM. Furthermore, additional tensile tests of the 2000 rpm-joint were performed up to different stress levels of near yield stress (YS), 70 pct UTS, and 95 pct UTS to analyze the deformation mechanisms.

III. RESULTS

A. Microstructural Characteristics

Figure 1 shows the microstructure of the parent material (PM). The as-received AZ31 shows a typical rolling microstructure with twins and inhomogeneous grains (Figure 1(a)). The average grain size was determined to be about 20 μm , and the number fraction of high-angle grain boundaries (HAGBs) was estimated to be 94.3 pct based on the EBSD analyses (Figure 1(b)). Furthermore, there are two prominent peaks in the misorientation angle distribution in Figure 1(b), which is quite different from a random distribution of the HCP crystallites.^[20] The first peak appears at $30 \pm 5^\circ$ and the second peak at $86 \pm 5^\circ$, which are related to the basal fiber texture^[21] and $\{10\bar{1}2\}$ twin boundaries,^[22] respectively. A strong rolling texture was found in the PM, with the (0002) normal nearly parallel to the ND (Figure 1(c)).

Figure 2 shows the macroscopic images of the transverse cross sections of the FSW AZ31 joints at different rotation rates. At 800 rpm, the NZ exhibited a basin shape (Figure 2(a)). At 2000 rpm, the NZ changed to an elliptical shape (Figure 2(b)). At 3500 rpm, a two-layer structure was clearly observed in the NZ (Figure 2(c)). In this study, these two regions in this two-layer-structured NZ were denoted by the upper and the lower zones, respectively. Specifically, the lower zone in the NZ bottom at 3500 rpm was elliptical and similar to the shape of the NZ at 2000 rpm. It is noted that the upper zone could be hardly observed at 800 rpm (Figure 2(a)), and it was a thin layer at 2000 rpm (Figure 2(b)). However, at 3500 rpm, the upper zone expanded downward significantly, with the area roughly equivalent to that of the lower zone.

Table I. Rotation Rates Used in This Study and Grain Sizes in Various Zones of FSW AZ31 Joints

Sample	Rotation rate (rpm)	Grain size in NZ (μm)	Grain size in TMAZ (μm)
800 rpm-joint	800	18.7	16.7
2000 rpm-joint	2000	23.3	16.4
3500 rpm-joint	3500	25.3 (upper zone) 17.9 (lower zone)	16.5

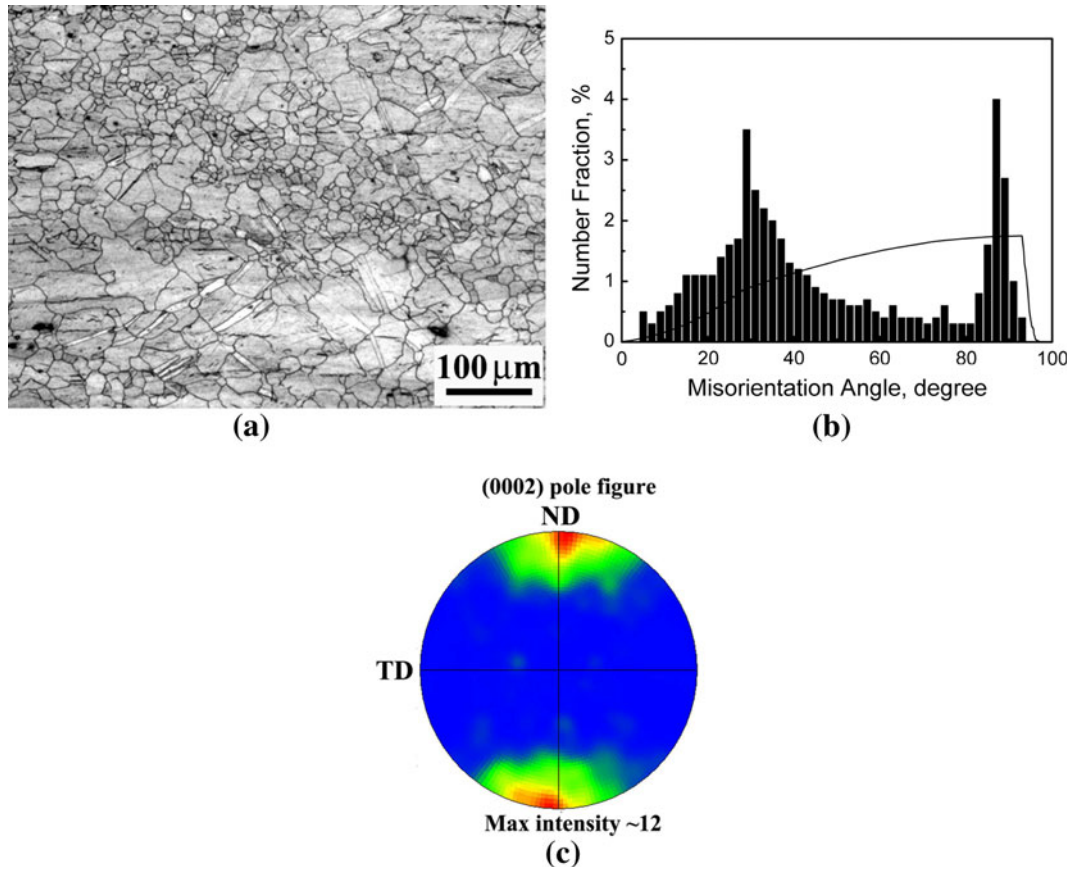


Fig. 1—Characteristic microstructural features of the PM: (a) optical image, (b) boundary misorientation distribution, and (c) (0002) pole figure.

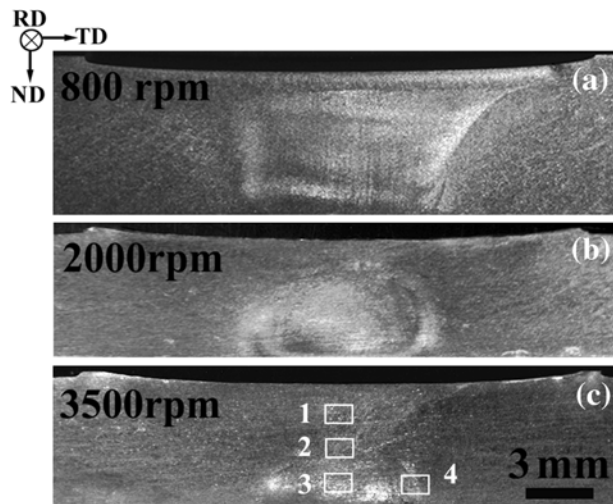


Fig. 2—Macroscopic images of the transverse cross section of the FSW AZ31 joints at different rotation rates (the advancing side is on the right).

For the 800 rpm-joint, equiaxed grain structures with average grain sizes of ~ 18.7 and $16.7 \mu\text{m}$ were, respectively, observed in the NZ (Figure 3(a)) and TMAZ (Figure 3(b)), with no twins appearing under OM. In the NZ center, the orientation discrepancies between different grains were small (Figure 3(c)), with the c-axis being

nearly parallel to the RD. However, the grain orientation had obvious variation at the NZ/TMAZ boundary (Figure 3(d)). While the grains in the NZ side at the NZ/TMAZ boundary were significantly rotated compared with that in the NZ center, and the grain orientations in the TMAZ side were more dispersive. For the 2000 rpm-joint, the average grain size increased to $23.3 \mu\text{m}$ in the NZ, but did not change ($16.4 \mu\text{m}$) in the TMAZ (Figure 4), and no twins were observed under OM. Moreover, the grain orientations in the NZ and TMAZ at 2000 rpm (not shown) were found to be similar to that at 800 rpm. For the 3500 rpm-joint, the grains in the upper zone of the NZ were coarse and roughly elongated along the TD (Figure 5(a)), while the grains in the lower zone were equiaxed and smaller (Figure 5(b)), with an average grain size of $17.9 \mu\text{m}$. No twins were observed in both zones of the NZ. The microstructure in the TMAZ (region 4 in Figure 2(c)) consisted of equiaxed grains with an average size of $16.5 \mu\text{m}$ (Figure 5(c)).

Figure 6 shows the boundary misorientation distributions in different regions at 800 and 3500 rpm. Similar misorientation distributions were found in the NZ at 800 rpm (Figure 6(a)) and in the lower zone of the NZ at 3500 rpm (Figure 6(c)). Compared to that in the PM, the peak of the misorientation angle at $86 \pm 5^\circ$ decreased significantly. Besides, most grains had the misorientation angles between 5° and 30° . However, the misorientation distributions were different between

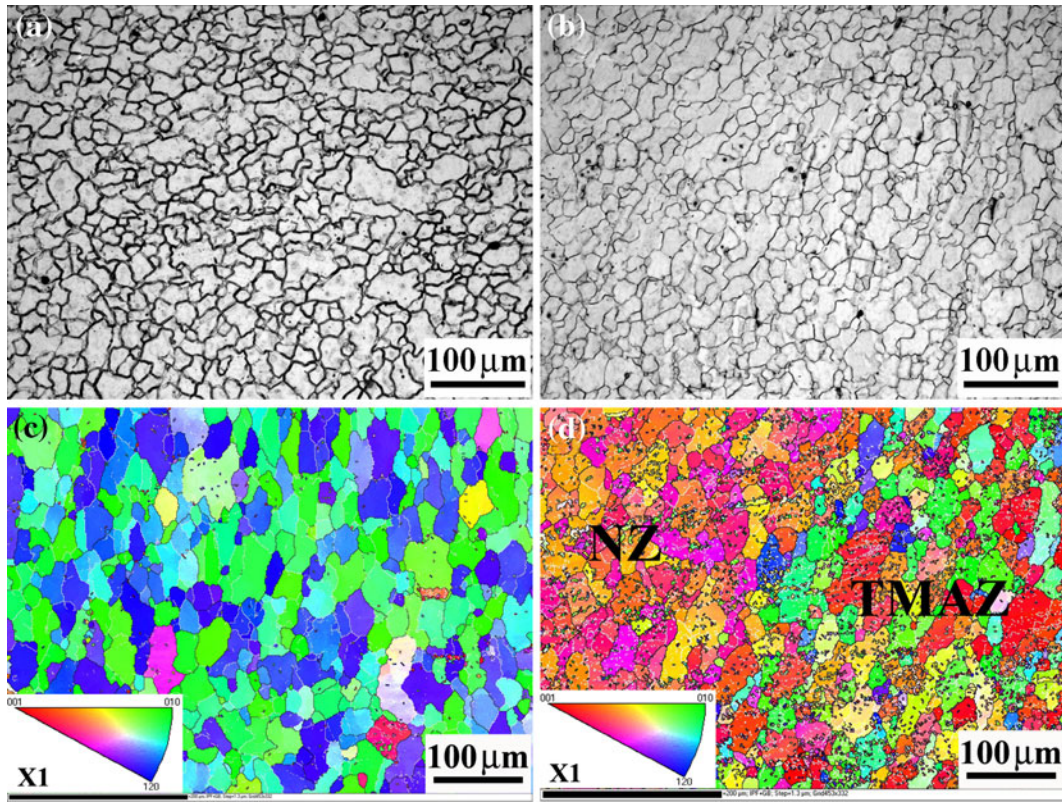


Fig. 3—Microstructure of the 800 rpm-joint: (a) and (b) optical microstructures in the NZ and TMAZ; (c) and (d) EBSD inverse pole figure maps in the NZ middle and at the NZ/TMAZ boundary.

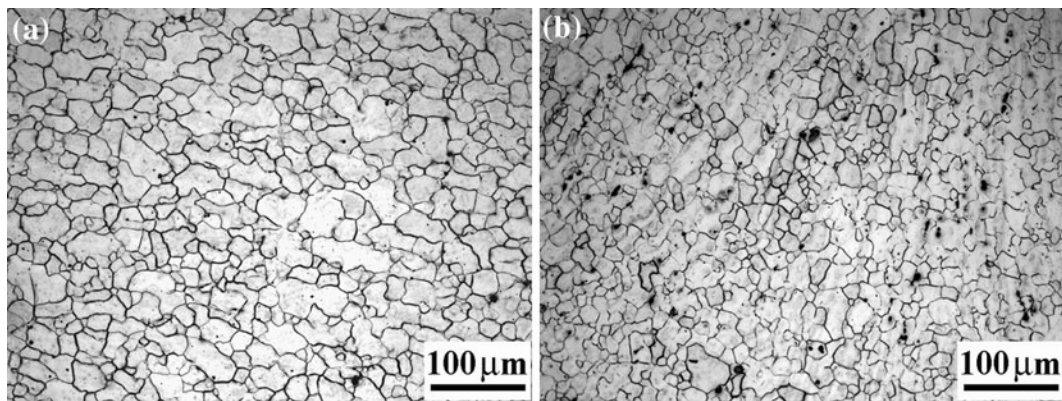


Fig. 4—Optical microstructures of the 2000 rpm-joint: (a) the NZ and (b) the TMAZ.

the upper zone (Figure 6(b)) and lower zone (Figure 6(c)) at 3500 rpm. The number fractions of HAGBs were 82 and 73.2 pct for the upper and lower zones, respectively. Furthermore, a strong peak at $30 \pm 5^\circ$ with a number fraction of 23.3 pct was observed in the upper zone, while the number fraction of misorientation angle at $30 \pm 5^\circ$ was 32.1 pct in the lower zone.

B. Texture Distribution

Figure 7 shows the (0002) pole figures of different regions in various FSW AZ31 joints. For the 800 rpm-joint, the texture of (0002) normal parallel to the RD

was found in the NZ center, and in the TMAZ, the basal plane being found tilted $\sim 34^\circ$ to the TD (Figure 7(a)). A similar texture distribution was found in the 2000 rpm-joint (Figure 7(b)). For the 3500 rpm-joint (Figure 7(c)), in the center of the upper zone (region 1), the basal plane was inclined $\sim 63^\circ$ to the ND and 71° to the RD. Compared with the PM, the basal plane in the upper zone tilted a little less. However, in the center of the lower zone (region 3), the normal of the basal plane was parallel to the RD, which was similar to those in the NZ centers at 800 and 2000 rpm. Furthermore, the transition region (region 2) between the upper and lower zones had the texture between the two zones with an

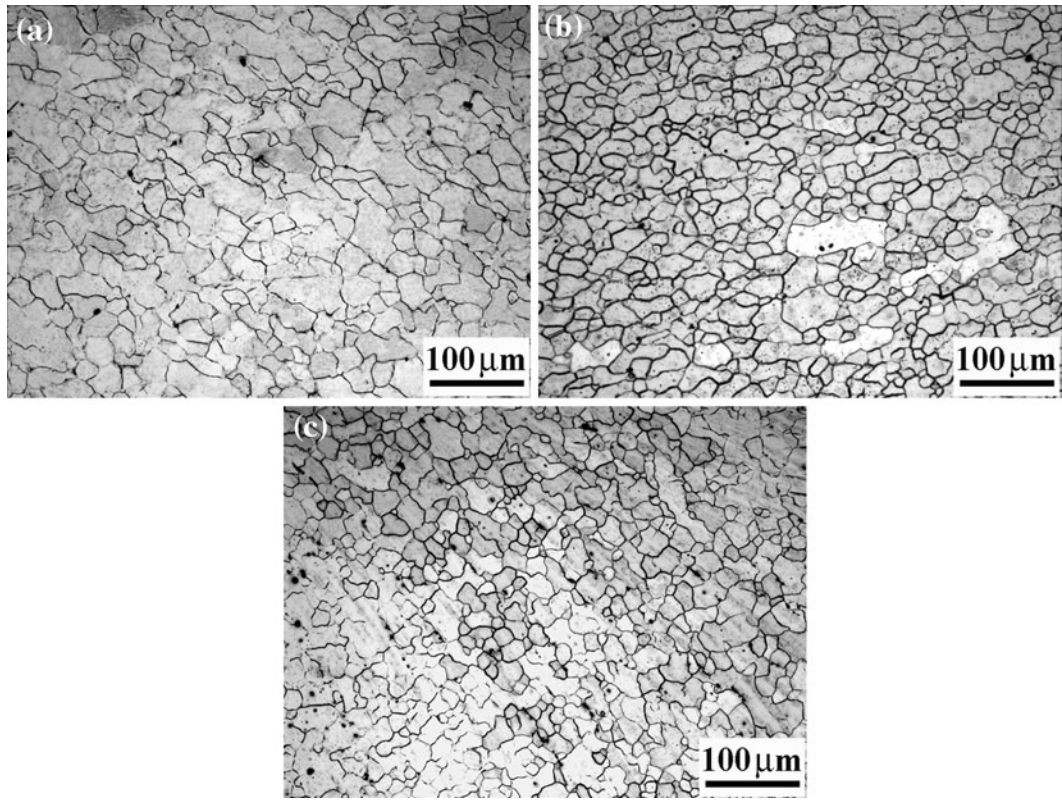


Fig. 5—Optical microstructures of the 3500 rpm-joint: (a) the upper zone, (b) the lower zone, and (c) the TMAZ.

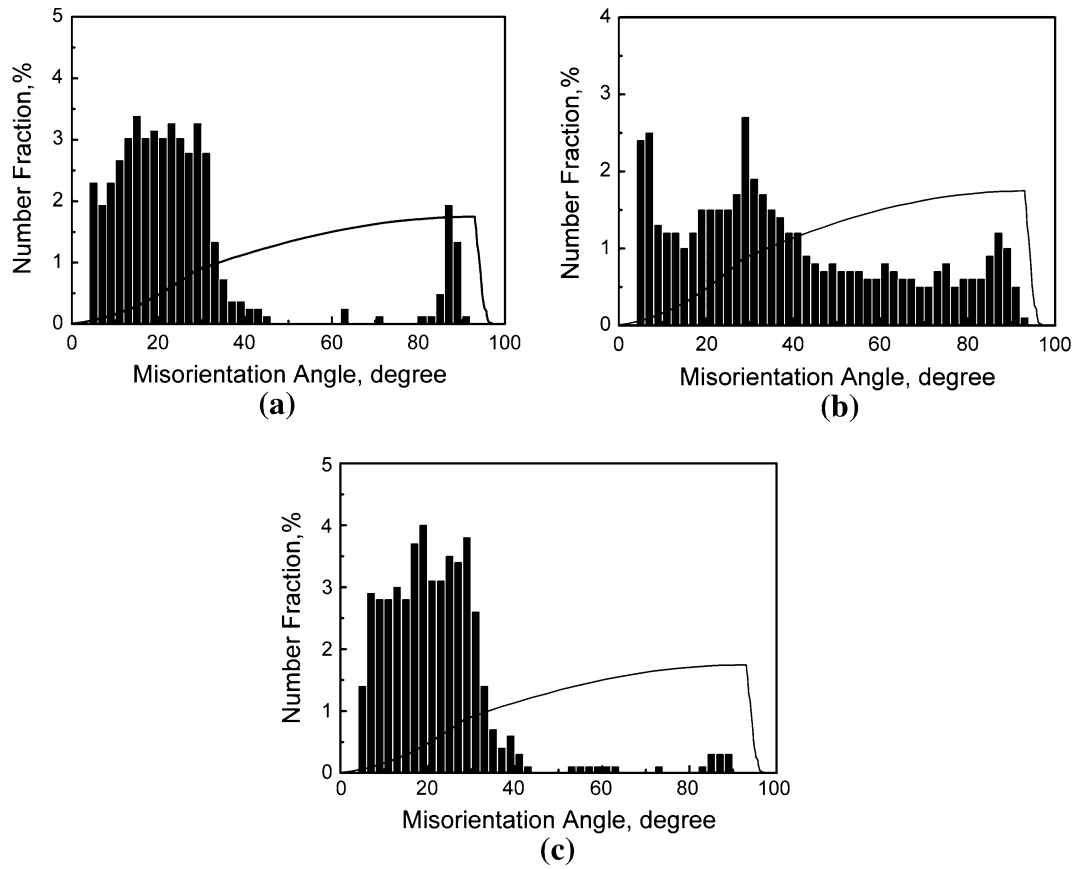


Fig. 6—Boundary misorientation distribution at different rotation rates: (a) the NZ at 800 rpm, (b) the upper zone, and (c) the lower zone at 3500 rpm.

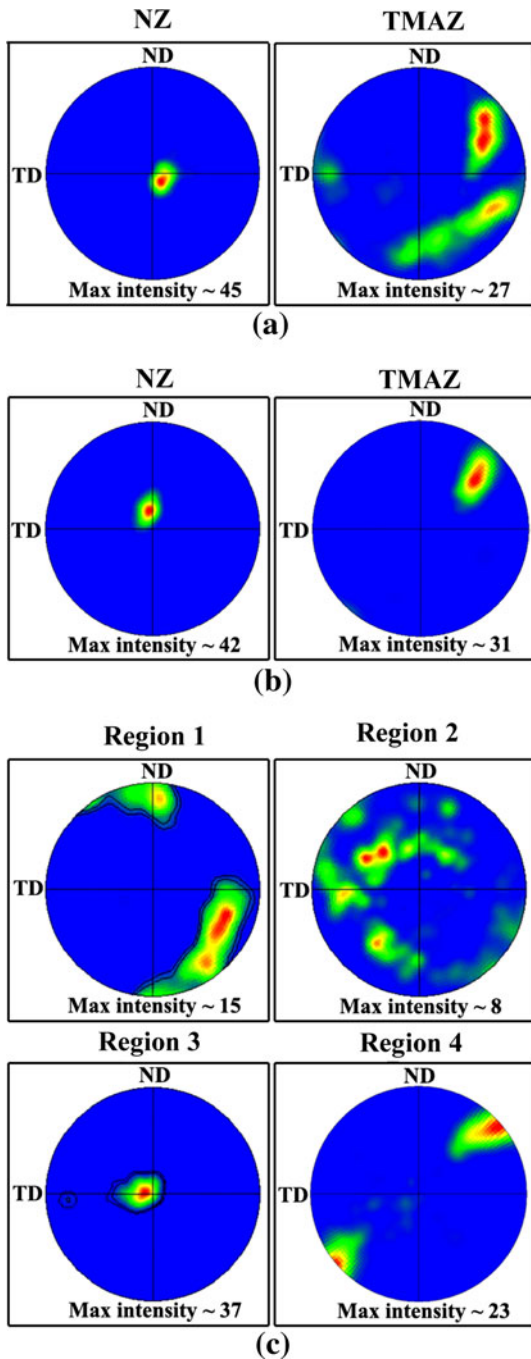


Fig. 7—The (0002) pole figures at different rotation rates: (a) the NZ and TMAZ at 800 rpm, (b) the NZ and TAMZ at the 2000 rpm, (c) regions 1-4 (shown in Fig. 2(c)) at 3500 rpm).

angle $\sim 38^\circ$ to the TD and $\sim 54^\circ$ to the RD. In the TMAZ (region 4), the angle between the basal plane and the TD was $\sim 41^\circ$. Therefore, compared with that in the PM, the texture in the lower zone was more intensively changed than that in the upper zone.

C. Tensile Deformation and Fracture Behavior

Figure 8 shows the microstructures of different regions in the 2000 rpm-joint deformed to different

stress levels. At a stress level of near the YS, the grain size in the NZ middle had little variation compared with the original grains, and almost no twins were observed (Figure 8(a)). However, obvious twinning was induced at the NZ/TMAZ boundary (Figure 8(b)). At a stress level of 75 pct UTS, few twins were found in the NZ middle with little variation of the grain size (Figure 8(c)); however, the twin density increased significantly at the NZ/TMAZ boundary (Figure 8(d)). It was noted that more twins were found in the NZ side than that in the TMAZ side of the NZ/TMAZ boundary, when the stress levels were near the YS and at 75 pct UTS (Figures 8(b) and (d)). Before the fracture (a stress level of 95 pct UTS), a large number of twins were detected in the NZ middle, which were thin, straight and long (Figure 8(e)). Furthermore, the twinning developed from the grains at the NZ/TMAZ boundary to the grains in the adjacent NZ gradually (Figure 8(f)). It is important to note that the twins at the NZ/TMAZ boundary were almost the same type at different stress levels, and they were irregular, chunky, and coarse.

Figure 9 shows the EBSD images of the specimen deformed to a stress level of 95 pct UTS. The twin boundaries in the NZ middle were identified as compression twins and double twins, marked by the red and green lines, respectively (Figure 9(a)). However, only tensile twin boundaries, marked by the blue line, were detected at the NZ/TMAZ boundary (Figure 9(b)).

Figure 10 shows the macroscopic images of the failed joints at different rotation rates. As shown in Figure 10(a), plane A and plane B are the two sides of a transverse tensile specimen, where the pin passed plane A earlier than plane B during the FSW process. In the uniaxial tension, the cracks did not propagate along a straight line (Figures 10(b) and (c)). For the 800 rpm-joint, the fracture location was at the NZ middle in plane A and the NZ/TMAZ boundary in plane B (Figure 10(b)). Similar fracture behavior was found in the 2000 rpm-joint (Figure 10(c)). However, a different fracture mode was found for the 3500 rpm-joint (Figure 10(d)), with similar fracture locations in plane A and plane B. The tensile specimen exhibited a 42° fracture in the upper zone, while the crack was curved toward the NZ/TMAZ boundary in the lower zone.

D. Mechanical Properties

Figure 11 shows the hardness profiles along the mid-thickness of the FSW AZ31 joints. As the rotation rate increased from 800 to 3500 rpm, the hardness profiles had little variation. There was little difference of hardness values between the NZ and PM. Hardness values fluctuated between 50 and 60 Hv.

Table II shows the mechanical properties of the FSW AZ31 joints. It was found that the UTS increased as the rotation rate increased. The joint efficiency was only 86.4 pct at 800 rpm, while it increased to the highest value of 95.2 pct at 3500 rpm. However, the variations of YS and elongation with the rotation rate were different from that of the UTS. The YS was about 104 MPa at 800 rpm, and then decreased to 92 MPa at 2000 rpm, and finally increased to 117 MPa at

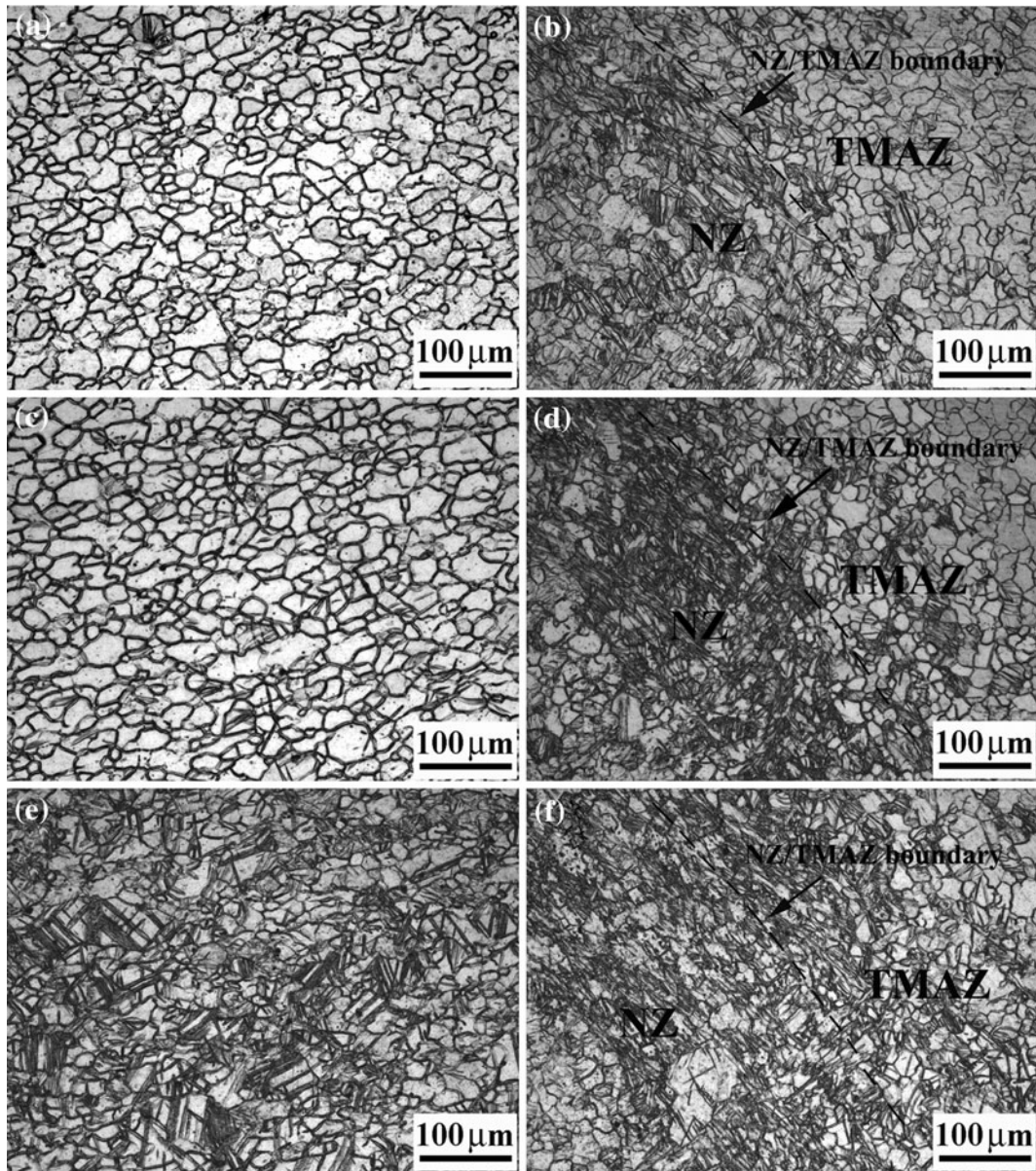


Fig. 8—Optical microstructure of the 2000 rpm-joint tensile deformed to different stress levels: (a) and (b) the NZ middle and NZ/TMAZ boundary near YS, (c) and (d) the NZ middle and NZ/TMAZ boundary at 75 pct UTS, (e) and (f) the NZ middle and the NZ/TMAZ boundary at 95 pct UTS.

3500 rpm. The elongation had little variation at different rotation rates. Furthermore, through the mini tensile test of the 3500 rpm-joint, the UTS of the upper zone was about 255 MPa, and higher than that of the lower zone (243 MPa).

Figure 12 shows the fractographs of the FSW AZ31 joints. Both the tear ridge and cleavage plane were observed on the fracture surfaces. However, the tear ridges were extended along different directions at various rotation rates. For the 800 rpm-joint and 2000 rpm-joint, the tear ridges were roughly along the ND (Figures 12(a) through (c)). However, different directions were found for the 3500 rpm-joint, with a clear boundary between the upper and lower zones (Figure 12(d)). The tear ridges were along the TD in the upper zone (Figure 12(e)), while they tended to extend

along the ND in the lower zone (Figure 12(f)). Moreover, the areas of the zones with the transverse and perpendicular tear ridges were equivalent, being similar to the microstructure distribution (Figure 2(c)).

IV. DISCUSSION

A. Nugget Shape Variation

An FSW tool, consisting of a shoulder and a pin, has two primary functions: heating the workpieces and driving the material flow.^[1] During FSW process, the heat is generated by the friction between the shoulder and the workpieces and by the plastic deformation around the tool. It is generally accepted that the former

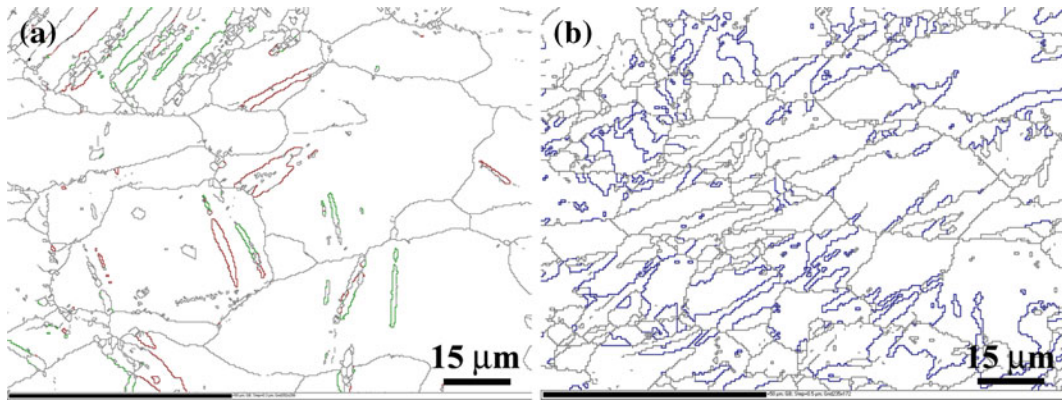


Fig. 9—EBSD images of the 2000 rpm-joint tensile deformed to 95 pct UTS at different regions: (a) the NZ middle (the compression twin boundaries $(56 \langle 1210 \rangle \pm 5^\circ)$ in red, the double twin boundaries $(38 \langle 1210 \rangle \pm 5^\circ)$ in green), (b) the NZ/TMAZ boundary (the tensile twin boundaries $(86 \langle 1210 \rangle \pm 5^\circ)$ in blue) (Color figure online).

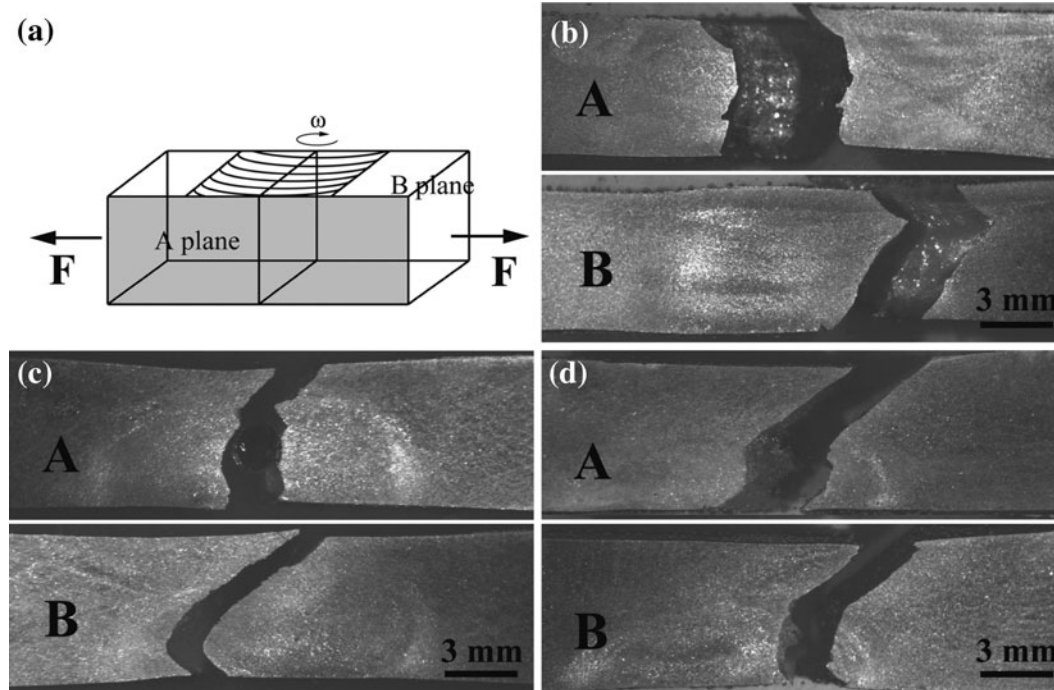


Fig. 10—(a) Schematic diagram of tensile specimens, (b) to (d) fracture locations at 800 rpm, 2000 rpm, and 3500 rpm, respectively (the advancing side is on the right).

one produced the most of the heat energy generated. The heat input (produced by the shoulder) per unit area and time was given by Frigaard *et al.*^[23]:

$$q_0 = \frac{4}{3} \pi^2 \mu P N R^3 \quad [1]$$

where N is the rotation rate, and R is the shoulder radius. Thus, the heat input from the shoulder increased with the rotation rate proportionately. Besides, the shoulder could cause deformation of materials on the plate surface by the rotation effect.^[12]

The nugget shape variation was related to the shoulder effect. The NZ usually consists of two parts: the upper zone and the lower zone, which were also defined as the shoulder-driven zone and pin-driven zone,

respectively, in FSW aluminum alloys.^[24,25] Arbegast^[26] found that a basin-shaped nugget was formed at a low rotation rate because of a thin shoulder-driven zone, whereas an elliptical nugget was produced at a higher rotation rate because of a slightly larger shoulder-driven zone. A similar result was observed in this study, as the rotation rate increased from 800 to 2000 rpm (Figures 2(a) and (b)). It is noted that the upper zone expanded to almost half of the NZ at 3500 rpm (Figure 2(c)), which was different from other studies at the rotation rates of 400-2000 rpm.^[27,28] At the lower rotation rate, the shoulder effect on the material flow was mainly restricted to the narrow near-surface layer.^[29] In this study, the formation of a two-layer structured NZ should be related to the high rotation rate.

At a high rotation rate of 3500 rpm, much larger heat input, based on Eq. [1], led to a high temperature in the upper zone, and further, a low heat-dissipation rate was produced in the upper zone for a thicker plate of 6.3 mm. Thus, the area of the upper zone with the high temperature expanded downward, which was proved by the simulation of temperature field in the FSW joints.^[30] Besides, the extrusion effect of the shoulder was more significant in this soft region. Therefore, the region affected by the shoulder changed from a narrow near-surface layer to an area roughly equal to the lower zone at 3500 rpm.

B. Grain Characteristics

As shown in Figures 3 through 6, the grains characteristics in the NZs at 800 and 2000 rpm were similar to those in the lower zone of the NZ at 3500 rpm. This indicates that similar recrystallization mechanisms operated in these regions, leading to the equiaxed grains and the similar boundary misorientation distributions (Figures 6(a) and (c)). The peak of misorientation angle at $86 \pm 5^\circ$ decreased significantly compared to that in the PM, which was consistent with the previous study of FSW AZ31^[11] and attributed to the high temperature [~ 673 K ($\sim 400^\circ\text{C}$)]^[5] and high strain^[31,32] during FSW process. Besides, most grains had misorientation angles between 5 and 30° , which was consistent with the FSW AZ31^[11] and friction stir-processed (FSP) AZ31.^[12] This specific nature of misorientation distribution was attributed to the texture:^[11] the grains were rotated around the $\langle 0001 \rangle$ direction in the NZ, and the maximal rotation angle was limited to 30° because of the symmetry of the HCP crystal structure.

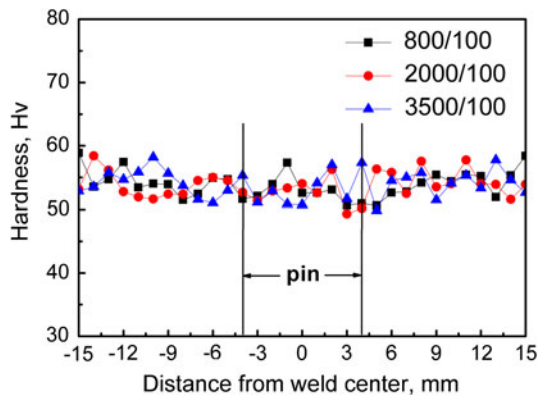


Fig. 11—Hardness profiles along the mid-thickness of the joints at different rotation rates (the advancing side is on the right).

However, the average grain size varied in the NZs at 800 and 2000 rpm and in the lower zone of the NZ at 3500 rpm (Table I). The largest grain size was obtained at 2000 rpm. Then, the grain size decreased at 3500 rpm (the lower zone) and was close to that at 800 rpm. This variation should be attributed to the change in the heat input and plastic deformation. The Zener-Hollomon parameter is usually used to analyze the strain rate and temperature during dynamic recrystallization. The equation is

$$Z = \dot{\epsilon} \exp(Q/RT) \quad [2]$$

where $\dot{\epsilon}$ is the strain rate, Q is the activation energy for lattice diffusion (a constant for AZ31 alloy), and RT has its usual meaning.

In Eq. [2], only the strain rate and temperature varied at different rotation rates. Chang *et al.*^[35] reported that the temperature in the NZ of FSP AZ31 increased as the rotation rate increased, and then it nearly remained stable with the rotation rate higher than 2000 rpm. However, the strain rate was reported to increase with the rotation rate.^[32] Therefore, it can be inferred that the Z parameter decreases as the rotation rate increases from 800 to 2000 rpm, and then increases when the rotation rate reaches 3500 rpm. In the FSP AZ31, the relationship between the grain size and the Z parameter was estimated by $\ln d = 9.0 - 0.27 \ln Z$,^[33] with the standard deviation for the grain size being less than $1.4 \mu\text{m}$. In this study, the grain size differences was about $4.6 \mu\text{m}$ between the NZs at 800 rpm and 2000 rpm, and about $5.4 \mu\text{m}$ between the NZ at 2000 rpm and the lower zone at 3500 rpm, indicating that it was suitable to use the Z parameters to analyze the grain size variation. The largest grain size at 2000 rpm could be attributed to the small Z value, while the smaller grain sizes at 800 and 3500 rpm were related to the larger Z value.

Equiaxed grains were observed in the TMAZ of the FSW AZ31 of the current study, which could be attributed to the dynamic recrystallization.^[9] At different rotation rates, the grains in the TMAZs were smaller than those in the NZ because of the lower temperature in the TMAZ.^[5] Besides, the grain size in the TMAZ varied little at different rotation rates, which was attributed to a weak dependence of the heat input^[34] and plastic deformation on the rotation rate in the TMAZ. In particular, the plastic deformation in the TMAZ was much weaker than that in the NZ and thus it could be conjectured that the strain in the TMAZ varied little at different rotation rates.

It should be noted that the grain structures were different between the upper and lower zones in the 3500 rpm-joint, which could be attributed to the

Table II. Transverse Tensile Properties of FSW AZ31 Joints at Different Rotation Rates

Sample	YS (MPa)	UTS (MPa)	El (pct)	Joint efficiency (pct)
800 rpm-joint	104.0 ± 0.8	215.6 ± 0.5	10.7 ± 0.7	86.4
2000 rpm-joint	92.1 ± 0.5	221.2 ± 1.1	10.6 ± 0.8	88.7
3500 rpm-joint	117.1 ± 2.0	237.5 ± 2.0	10.8 ± 0.9	95.2

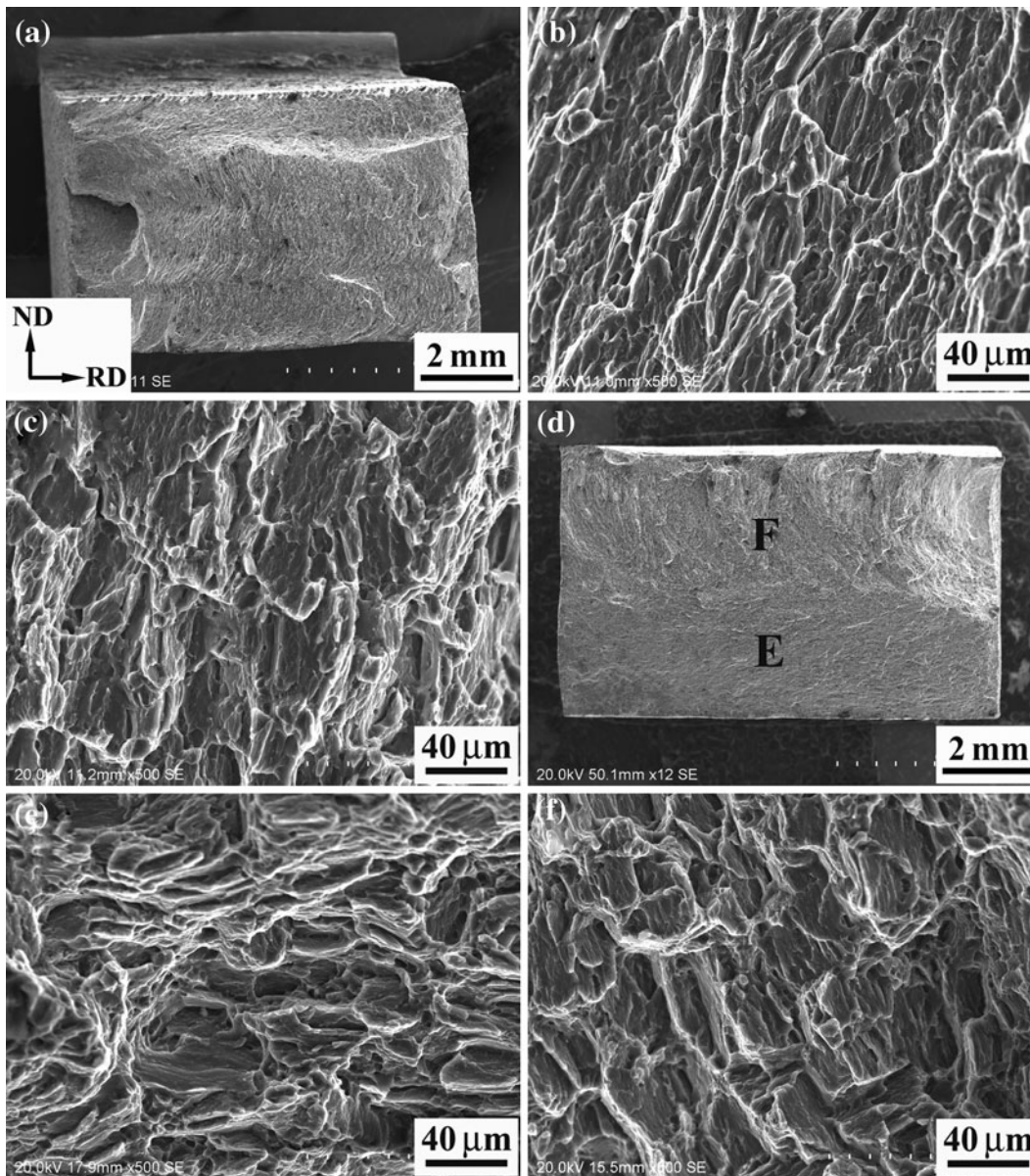


Fig. 12—SEM fractographs of FSW AZ31 joints: (a) macrograph at 800 rpm; (b) and (c) micrographs at 800 and 2000 rpm; (d) macrograph at 3500 rpm; (e) and (f) micrographs of the upper zone (region E) and lower zone (region F) at 3500 rpm.

different temperatures and deformations during FSW process. As discussed above, the formation of the equiaxed grain in the lower zone was due to the dynamic recrystallization. However, the temperature in the upper zone was higher than that in the lower zone, leading to the coarse grains in the upper zone (Figure 5(a)). Besides, during the FSW process, the extrusion effect was exerted on the upper zone by the shoulder,^[1] thus causing the grains to be elongated along the TD.

Because of the existence of the extrusion effect, the deformation in the upper zone was different from that in the lower zone, and hence a different boundary misorientation distribution was produced (Figure 6(b)). It was reported that the deformation could induce the transformation of the twin boundaries into random HAGBs^[11,35] because of the crystallographic rotations. Therefore, the peaks of $86 \pm 5^\circ$ boundaries in the upper

zone were lower than those in the PM (Figures 1(b) and 6(b)). On the other hand, this extrusion effect made the boundary misorientation with intense peaks of $30 \pm 5^\circ$ boundaries similar to that in the PM. In the lower zone (Figure 6(c)), the characteristic misorientation distribution was found with most grain boundaries (89 pct) in the range of $5\text{--}30^\circ$, thus the misorientation angle at $30 \pm 5^\circ$ (32.1 pct) was part of this range rather than the distinctly intense peak.

C. Texture Distribution

The schematic evolution of the basal plane is shown in Figure 13. Two types of texture distribution were found in the FSW AZ31 joints at different rotation rates. The first one was observed in the 800 rpm-joint and 2000 rpm-joint. As shown in Figures 7(a) and (b), the

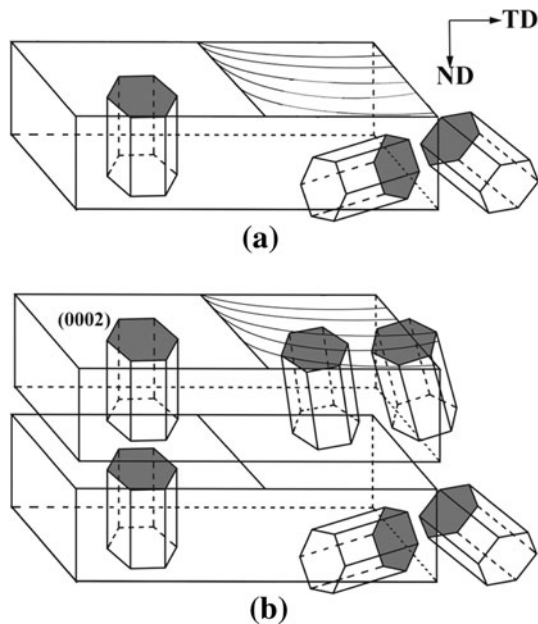


Fig. 13—Schematic of evolutions of basal planes in the FSW AZ31 joints at different rotation rates: (a) 800 and 2000 rpm, (b) 3500 rpm.

basal plane was perpendicular to the normal plane in the NZ middle, while it was tilted to the TD at an angle of $\sim 40^\circ$ in the TMAZ. Park *et al.*^[17] measured the pole figures at different regions of the FSW AZ61 and suggested that the basal plane in the NZ roughly surrounded the pin column surface. Similar texture distribution was also reported in AZ31 by Woo *et al.*^[10] In the current study, textures in the specific locations (NZ middle and TMAZ) were consistent with the previous study.^[17] Besides, the NZ shape and rotation rates in this study were similar to those in the previous studies.^[10,17] Therefore, the (0002) basal planes are parallel to the pin column surface in the NZ at 800 and 2000 rpm (Figure 13(a)).

A different type of texture distribution was detected in the 3500 rpm-joint. In the two-layer structured NZ, the texture distribution in the lower zone was similar to those in the NZs at 800 and 2000 rpm, with the basal planes being parallel to the pin surface (Figure 13(b)). As discussed above, the extrusion effect from the shoulder was exerted on the softened material in the upper zone; thus, the basal plane was no longer rotated (Figure 7(c)). Therefore, the basal plane in the upper zone inclined somewhat compared to that in the PM (Figure 13(b)). Similar texture evolution was also found in the thin top surface of FSW AZ31 joint at a low rotation rate^[17] and in the whole NZ of FSP AZ31 using a very short and small pin.^[19] It can be concluded that this texture evolution resulted from the shoulder effect, and thus the high rotation rate and small pin are conducive to this texture evolution.

In summary, the texture distribution in the NZs was related to the rotation rate. At 800 and 2000 rpm, the upper zone was only a thin layer, and thus the column-rotated basal plane was the main texture distribution of the NZ. However, at 3500 rpm, with the expansion of

the upper zone, the texture in the upper zone became more significant, which would exert a significant effect on the mechanical properties of the joint (this will be discussed in Sections IV-D and IV-E).

D. Fracture Behavior

Two types of fracture behaviors were found in the transverse tensile specimens of the FSW AZ31 joints. The first one (fracture type I) was found in the 800 rpm-joint and 2000 rpm-joint: the fracture location was at the NZ middle in plane A and the NZ/TMAZ boundary in plane B (Figures 10(b) and (c)). The second one (fracture type II) was detected in the 3500 rpm-joint, where similar fracture behaviors were found in planes A and B, with the fracture path inclined about 42° to the tensile direction in the upper zone and warped toward the NZ/TMAZ boundary in the lower zone (Figure 10(d)). However, in the hardness profiles (Figure 11), there was no obvious lowest hardness region. Therefore, other factors should be responsible for different fracture behaviors.

1. Fracture type I

For fracture type I, it can be concluded that two weak regions, the NZ/TMAZ boundary and the NZ middle, existed in the joints, based on Figures 10(b) and (c). The weak region at the NZ/TMAZ boundary was related to the texture distribution. Many studies^[17,18] pointed out that the material in the TMAZ were prone to deforming and failing because of soft orientation with $\sim 45^\circ$ inclination between the basal plane and the tensile direction. The similar orientation in the TMAZ was found in the current study (Figure 7), which could cause the failure. Another reason for the fracture should be the non-uniform plastic deformation at the NZ/TMAZ boundary. Although a similar suggestion was also given by Woo *et al.*,^[10] detailed study was lacking. As shown in Figures 3(d) and 7(a), the basal plane in the TMAZ side was tilted $\sim 60^\circ$ compared to that in the NZ side. Furthermore, a higher Schmid factor (0.4-0.5) was observed in most grains in the NZ side, while the lower Schmid factor (about 0.2) was detected for the grains in the TMAZ side (Figure 14). This indicates that the grains in the NZ side were prone to deforming at an early stage during the tension.

The non-uniform deformation at the NZ/TMAZ boundary was revealed by the twin evolution during the tension (Figure 8). At a stress level of near Y_S , a large number of twins were formed in the NZ side, while few twins were found in the TMAZ side (Figure 8(b)). These irregular, chunky, and coarse twins were identified as the tensile twins (Figure 9(b)), which observation was consistent with other studies.^[36,37] However, the twinning was often observed in the grains after yielding in the AZ31 sheet.^[36] In this study, because the grains in the NZ side had the higher Schmid factor, the basal slip occurred early at a lower stress. Then, the anisotropic stress concentration emerged, and the tensile twins were formed to accommodate the concentrated stresses before the yield. It could be inferred that the microscopic yielding occurred in the NZ side at a lower stress.

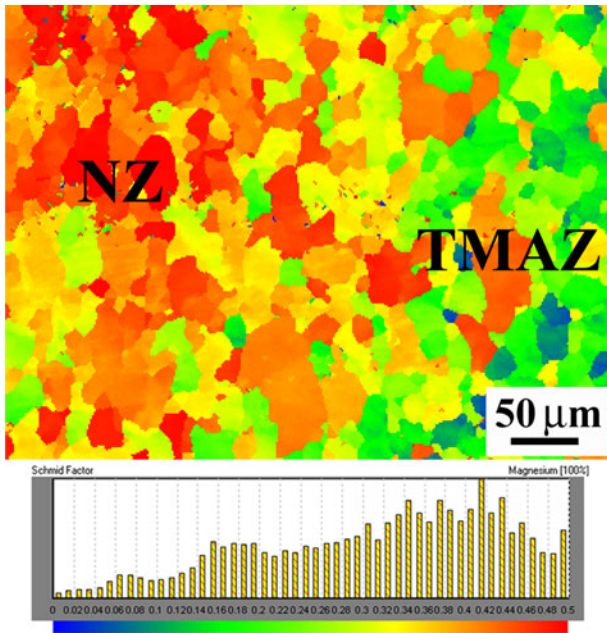


Fig. 14—EBSD Schmid factor analysis for basal slip at the NZ/TMAZ boundary at 2000 rpm.

When the stress reached 75 pct UTS, most regions experienced plastic deformation, but the deformation was still non-uniform (Figure 8(d)). At this stress level, the twinning was an important deformation mechanism.^[36] In the tensile specimen, the twin density decreased from the NZ/TMAZ boundary to the NZ interior because of the column-rotated basal plane. At the NZ/TMAZ boundary, a higher twin density was found in the NZ side than in the TMAZ side, indicating that the adjacent NZ was easier to deform. Therefore, the existence of the weak zone at the NZ/TMAZ boundary was due to the orientation favoring deformation and the incompatible deformation.

The other weak zone was the NZ middle. At the stress levels of near YS (Figure 8(a)) and 75 pct UTS (Figure 8(c)), little deformation was observed in the NZ middle, with few twins and little variations of the grains compared with the original grains without deformation. It should be attributed to the texture distribution. During the tension, the (0002) normal was perpendicular to the tensile direction (Figure 7) in the NZ middle, and the Schmid factor was nearly zero for most grains, so that both the basal slip and tensile twin were difficult to activate. However, when the stress reached 95 pct UTS, a large number of compression twins and double twins were formed (Figures 8(e) and 9(a)), which was different from the tensile twins at the NZ/TMAZ boundary (Figure 9(b)).

The compression twinning is expected when a grain is in compression along the c-axis.^[38] As for the double twinning, it is generally known that the compression twins form first, and the tensile twins propagated within the original compression twins.^[39] In this study, when the specimen was subjected to uniaxial tension, there was a compression along both the thickness and width directions. Besides, the normal of the basal plane was

parallel to the RD in the NZ middle. Therefore, the compression strain was parallel to the c-axis, causing the compression twinning and double twinning. In contrast, the grains were oriented unfavorably for the compression twinning at the NZ/TMAZ boundary. Moreover, it was reported that the average value of critical resolved shear stress (CRSS) for the compression twinning is about 112 MPa,^[39] which is much higher than that for the tensile twinning (4 MPa).^[40] This explains the result that the compression twins were obviously observed only at the high stress (95 pct UTS).

Furthermore, there was an important relationship between the fracture and the compression twins. The role of the tensile twinning appeared to accommodate the stress concentration.^[36] However, the compression twins were reported to cause fracture.^[39–41] In the NZ middle, the formation of the compression twins and double twins could produce a highly localized shear-deformation region and lead to the strain incompatibility and the failure at the twin interface. Therefore, at 800 and 2000 rpm, the possible fracture mechanism was that: the crack originated at the NZ/TMAZ boundary because of the orientation favoring deformation and the incompatible deformation, and then it propagated to the NZ middle for the effect of the compression twinning and double twinning.

2. Fracture type II

For fracture type II found in the 3500 rpm-joint, similar fracture behaviors were found in planes A and B. This should be attributed to the two-layer structure of the NZ. Column-distributed basal plane was found in the lower zone, while a slightly tilted basal plane to that in the PM was found in the upper zone. Thus, the fracture behavior in the upper zone was similar to that in the PM, leading to the fracture along the plane with the highest shear stress. Consequently, the fracture path inclined $\sim 42^\circ$ to the tensile direction (Figure 10(d)). Furthermore, the upper zone expanded at 3500 rpm, and thus its effect on the fracture was more important. However, because of the texture distribution in the lower zone, the straight fracture line was warped toward the NZ/TMAZ boundary. Therefore, the mixed fracture was found in the tensile specimen.

E. Mechanical Properties

The hardness profiles had little variations at different rotation rates, with hardness value in the NZ equivalent to that in the PM. Similar hardness profiles were also found in the previous study of FSW AZ31,^[9] which were attributed to the hardness insensitivity to the grains size variation at a certain range.

As the rotation rate increased, the YS decreased slightly from 800 to 2000 rpm, and then increased at 3500 rpm (Table II). Both the grain size and texture could influence the YS. At 800 and 2000 rpm, the grain characteristic and the texture distribution of the NZs were similar, but grain coarsening was found in the NZ at 2000 rpm, and thus the lower YS was measured at 2000 rpm, with similar fracture locations in the NZ (Figures 10(b) and (c)). At 3500 rpm, the higher YS

could be related to the fine grains in the lower zone and the texture distribution in the upper zone. During the tension, the material in the lower zone tended to yield early for the column distributed basal plane, while the texture in the upper zone made the material yield at a higher stress. Therefore, a slightly higher YS was observed at 3500 rpm.

However, the UTS increased with the rotation rate (Table II). As the rotation rate increased from 800 to 2000 rpm, a slight UTS increase from 215.6 to 221.2 MPa was found. It could not be attributed to the grain size variation, because the grain size in the NZ increased. Because of the same fracture location at the NZ/TMAZ boundary (Figures 10(b) and (c)), the UTS increase should be related to the enhancement of this region. For the basin-shaped nugget at 800 rpm, the NZ/TMAZ boundary was roughly a straight line, which was $\sim 53^\circ$ to the tensile direction. Besides, the basal plane tilted $\sim 40^\circ$ to the TD in this region. Therefore, the NZ/TMAZ boundary was not only the plane with the highest shear stress for the geometry factor, but also prone to deforming for the texture factor. However, at 2000 rpm, only the texture factor operated because of the elliptical nugget. Consequently, a slightly higher UTS was observed at 2000 rpm.

At 3500 rpm, the highest joint efficiency of 95 pct was obtained, which should be attributed to the two-layer structure of the NZ. For the mini tensile test, the UTS of the upper zone were slightly larger than that in the lower zone. In the lower zone, the soft orientation was found in the TMAZ (Figure 7(c)). However, in the upper zone, no obvious soft region existed during the tension, because the basal plane only tilted at a small range compared to that in the PM. As a result, the upper zone had a higher tensile strength despite the coarse grains (Table I). Therefore, a higher tensile strength of the joint was achieved at 3500 rpm.

In the previous studies of FSW AZ31,^[2,5,6,9] a wide range of rotation rates (600-2500 rpm) were used to join rolled plates, but the joint efficiency was not as high as that in the present study. It was noted that the rotation rates in these studies were much lower than that in this study. Therefore, it could be inferred that high rotation rate is beneficial to improving the mechanical properties of the FSW AZ31 joint.

Both tear ridges and cleavage planes were observed on the fracture surface of the joints (Figure 12), indicating the quasi-cleavage fracture. The direction of the tear ridges may have some relation with the texture distribution. It was reported that the basal plane was the main habit plane of the cleavage in the HCP metals,^[38] which contributed to the lower critical fracture stress for Mode I slit cracks. In the NZs at 800 and 2000 rpm and the low zone at 3500 rpm, the basal plane was rotated around the pin column, and the orientation was different for each grain, forming the cleavage discontinuous distribution and the tear ridges roughly along the ND (Figures 12(b), (c) and (f)). However, at 3500 rpm, the basal plane in the upper zone inclined little to that in the PM, leading to the tear ridges almost along the TD (Figure 12(e)).

V. CONCLUSIONS

1. The NZ changed from basin to elliptical shape as the rotation rate increased from 800 to 2000 rpm at a constant welding speed of 100 mm/minutes. At 3500 rpm, the two-layer structure was obtained in the NZ, with the area of the upper zone equal to that of the lower zone.
2. Similar equiaxed fine grain structure was found in the NZ at 800 and 2000 rpm, and in the lower zone of the NZ at 3500 rpm. However, elongated coarse grains were observed in the upper zone of the NZ at 3500 rpm.
3. In the NZ at 800 rpm and the lower zone at 3500 rpm, the $\{10\bar{1}2\}$ twins almost disappeared with the misorientation angle between 5° and 30° for most grains. However, a strong peak at $30 \pm 5^\circ$ was observed in the upper zone, which was similar with that in the PM.
4. The column-rotated basal plane was the main texture distribution in the NZ at 800 and 2000 rpm and in the lower zone at 3500 rpm. However, the basal plane in the upper zone had little inclination compared to that in the PM at 3500 rpm.
5. Both the NZ middle and the NZ/TMAZ boundary were the weak zones during tension. The weak zone in the NZ middle was due to the compression twinning and double twinning at high stress level, while that at the NZ/TMAZ boundary resulted from the non-uniform deformation and $\sim 45^\circ$ inclination between the basal plane and the tensile direction.
6. At 800 and 2000 rpm, both the NZ middle and the NZ/TMAZ boundary were the fracture locations. However, at 3500 rpm, because of the enhancement of the upper zone, the tensile specimen exhibited a 42° fracture in the upper zone, while the crack was curved toward the NZ/TMAZ boundary in the lower zone.
7. The YS decreased with increasing the rotation rate from 800 to 2000 rpm for the grain coarsening in the NZ, and then it increased at 3500 rpm for the two-layer structure. Besides, the UTS increased with the rotation rate, with the highest joint efficiency of 95 pct at 3500 rpm, which was attributed to the variations in both the texture and nugget shape.

ACKNOWLEDGMENTS

This study was supported by the National R&D Program of China under grant No. 2011BAE22B05, the National Outstanding Young Scientist Foundation of China under grant No. 50525103, and the Hundred Talents Program of Chinese Academy of Sciences.

REFERENCES

1. R.S. Mishra and Z.Y. Ma: *Mater. Sci. Eng. R*, 2005, vol. 50, pp. 1-78.
2. W.B. Lee, Y.M. Yeon, and S.B. Jung: *Mater. Sci. Technol.*, 2003, vol. 19, pp. 785-90.

3. S. Lin, S. Kim, C.G. Lee, C.D. Yim, and S.J. Kim: *Metall. Mater. Trans. A*, 2005, vol. 36A, pp. 1906–12.
4. M.A. Gharacheh, A.H. Kokabi, G.H. Daneshi, B. Shalchi Amir-khiz, and R. Sarrafi: *Int. J. Mach. Tool Manuf.*, 2006, vol. 46, pp. 1983–87.
5. L. Commin, M. Dumont, J.E. Masse, and L. Barrallier: *Acta Mater.*, 2009, vol. 57, pp. 326–34.
6. N. Afrin, D.L. Chen, X. Cao, and M. Jahazi: *Mater. Sci. Eng. A*, 2008, vol. 472, pp. 179–86.
7. X.H. Wang and K.S. Wang: *Mater. Sci. Eng. A*, 2006, vol. 431, pp. 114–17.
8. J. Yang, D. Wang, B.L. Xiao, and Z.Y. Ma: *8th International Friction Stir Welding Symposium: Timmendorfer Strand, Germany*, 2010.
9. J. Yang, B.L. Xiao, D. Wang, and Z.Y. Ma: *Mater. Sci. Eng. A*, 2010, vol. 527, pp. 708–14.
10. W. Woo, H. Choo, D.W. Brown, P.K. Liaw, and Z. Feng: *Scripta Mater.*, 2006, vol. 54, pp. 1859–64.
11. U.F.H.R. Suhuddin, S. Mironov, Y.S. Sato, H. Kokawa, and C.W. Lee: *Acta Mater.*, 2009, vol. 57, pp. 5406–18.
12. S. Mironov, Q. Yang, H. Takahashi, I. Takahashi, K. Okamoto, Y.S. Sato, and H. Kokawa: *Metall. Mater. Trans. A*, 2010, vol. 41A, pp. 1016–24.
13. S. Mironov, Y. Motohashil, and R. Kaibyshev: *Mater. Trans.*, 2007, vol. 48, pp. 1387–95.
14. G.M. Xie, Z.Y. Ma, L. Geng, and R.S. Chen: *Mater. Sci. Eng. A*, 2007, vol. 471, pp. 63–68.
15. D.T. Zhang, M. Suzuki, and K. Maruyama: *Scripta Mater.*, 2005, vol. 52, pp. 899–03.
16. W.J. Kim, S.I. Hong, K.S. Kim, S.H. Min, H.T. Jeong, and J.D. Lee: *Acta Mater.*, 2003, vol. 51, pp. 3293–07.
17. S.H.C. Park, Y.S. Sato, and H. Kokawa: *Metall. Mater. Trans. A*, 2003, vol. 34A, pp. 987–94.
18. S.H.C. Park, Y.S. Sato, and H. Kokawa: *Scripta Mater.*, 2003, vol. 49, pp. 161–66.
19. W. Yuan, R.S. Mishra, B. Carlson, R.K. Mishra, R. Verma, and R. Kubic: *Scripta Mater.*, 2011, vol. 64, pp. 580–83.
20. M.Y. Wang, R.L. Xin, B.S. Wang, and Q. Liu: *Mater. Sci. Eng. A*, 2011, vol. 528, pp. 2941–51.
21. A.H. Feng and Z.Y. Ma: *Acta Mater.*, 2009, vol. 57, pp. 4248–60.
22. J.A. Del Valle, M.T. Perez-Prado, and O.A. Ruano: *Metall. Mater. Trans. A*, 2005, vol. 36A, pp. 1427–38.
23. Ø. Frigaard, Ø. Grong, and O.T. Midling: *Metall. Mater. Trans. A*, 2001, vol. 32A, pp. 1189–1200.
24. K. Kumar and S.V. Kailas: *Mater. Sci. Eng. A*, 2008, vol. 485, pp. 367–74.
25. Z. Zhang, B.L. Xiao, D. Wang, and Z.Y. Ma: *Metall. Mater. Trans. A*, 2011, vol. 42A, pp. 1717–26.
26. W.J. Arbegast: *Scripta Mater.*, 2008, vol. 58, pp. 372–76.
27. Y.S. Sato, H. Kokawa, M. Enomoto, and S. Jogan: *Metall. Mater. Trans. A*, 1999, vol. 34A, pp. 2429–37.
28. Z.Y. Ma, S.R. Sharma, and R.S. Mishra: *Mater. Sci. Eng. A*, 2006, vol. 433, pp. 269–78.
29. Z.W. Chen, T. Pasang, and Y. Qi: *Mater. Sci. Eng. A*, 2008, vol. 474, pp. 312–16.
30. X.X. Zhang, B.L. Xiao, and Z.Y. Ma: *Metall. Mater. Trans. A*, 2011, vol. 42A, pp. 3229–39.
31. M.M. Myshlyayev, H.J. McQueen, A. Mwembela, and E. Konopleva: *Mater. Sci. Eng. A*, 2002, vol. 337, pp. 121–33.
32. C.I. Chang, X.H. Du, and J.C. Huang: *Scripta Mater.*, 2007, vol. 57, pp. 209–12.
33. C.I. Chang, C.J. Lee, and J.C. Huang: *Scripta Mater.*, 2004, vol. 51, pp. 509–14.
34. F.C. Liu and Z.Y. Ma: *Metall. Mater. Trans. A*, 2008, vol. 39A, pp. 2378–88.
35. S.Y. Mironov, G.A. Salishchev, M.M. Myshlyayev, and R. Pippan: *Mater. Sci. Eng. A*, 2006, vol. 418, pp. 257–67.
36. J. Koike: *Metall. Mater. Trans. A*, 2005, vol. 36A, pp. 1689–96.
37. L. Jiang, J.J. Jonas, R.K. Mishra, A.A. Luo, A.K. Sachdev, and S. Godet: *Acta Mater.*, 2007, vol. 55, pp. 3899–10.
38. M.H. Yoo: *Metall. Mater. Trans. A*, 1981, vol. 12A, pp. 409–18.
39. B.C. Wonsiewicz and W.A. Backofen: *Trans. TMS-AIME*, 1967, vol. 239, pp. 1422–87.
40. R.E. Reedhill and W.D. Robertson: *Acta Metall*, 1957, vol. 5, pp. 717–27.
41. H. Yoshinag, T. Obara, and S. Morozumi: *Mater. Sci. Eng.*, 1973, vol. 12, pp. 255–64.